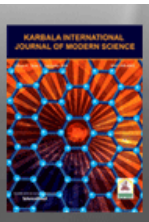

Karbala International Journal of Modern Science

Volume 8 | Issue 2 Article 9

Synthesis of CuO/ZnO and MgO/ZnO Core/Shell Nanoparticles with Plasma Jets and Study of their Structural and Optical Properties

Raghad S. Mohammed
Department of Physics, College of Science, Mustansiriyah University, Baghdad, Iraq,
raghad.almaliki@uomustansiriyah.edu.iq

Kadhim A. Aadim
Department of Physics, College of Science, University of Baghdad, Baghdad, Iraq

Khalid A. Ahmed
Department of Physics, College of Science, Mustansiriyah University, Baghdad, Iraq

Synthesis of CuO/ZnO and MgO/ZnO Core/Shell Nanoparticles with Plasma Jets and Study of their Structural and Optical Properties

Abstract

This paper reports the synthesis of CuO/ZnO and MgO/ZnO core/shell nanoparticles using atmospheric plasma jets. The characterization of the synthesized CuO/ZnO and MgO/ZnO core/shell nanoparticles were confirmed by a series of techniques, including X-ray diffraction (XRD), scanning electron microscopy (SEM), X-ray dispersive spectroscopy (EDS), transmission electron microscopy (TEM), and UV–Vis spectroscopy. The XRD analysis confirmed no other peaks related to the secondary phases for CuO, MgO, or ZnO, indicating the purity of these nanoparticles. Additionally, EDX analysis confirmed the formation of high purity CuO/ZnO and MgO/ZnO core/shell nanoparticles. The surface morphology, which represented the high agglomeration rate, was investigated using SEM. TEM analysis showed that the sizes of the CuO/ZnO and MgO/ZnO core/shell nanoparticles were 32 nm and 70 nm, respectively. The energy bandgaps were 3.3 eV and 3.1 eV for the CuO/ZnO and MgO/ZnO core/shell nanoparticles.

Keywords

Hybrid nanoparticles, Plasma jets, CuO/ZnO core/shell nanoparticles, MgO/ZnO core/shell nanoparticles, Structural properties, optical properties

Cover Page Footnote

Acknowledgements This study is supported by Plasma Physics Lab., Physics Department, College of Science, University of Baghdad

RESEARCH PAPER

Synthesis of CuO/ZnO and MgO/ZnO Core/Shell Nanoparticles with Plasma Jets and Study of their Structural and Optical Properties

Raghad S. Mohammed [a,*], Kadhim A. Aadim [b], Khalid A. Ahmed [a]

[a] Department of Physics, College of Science, Mustansiriyah University, Baghdad, Iraq
[b] Department of Physics, College of Science, University of Baghdad, Baghdad, Iraq

Abstract

This paper reports the synthesis of CuO/ZnO and MgO/ZnO core/shell nanoparticles using atmospheric plasma jets. The characterization of the synthesized CuO/ZnO and MgO/ZnO core/shell nanoparticles were confirmed by a series of techniques, including X-ray diffraction (XRD), scanning electron microscopy (SEM), X-ray dispersive spectroscopy (EDS), transmission electron microscopy (TEM), and UV−Vis spectroscopy. The XRD analysis confirmed no other peaks related to the secondary phases for CuO, MgO, or ZnO, indicating the purity of these nanoparticles. Additionally, EDX analysis confirmed the formation of high purity CuO/ZnO and MgO/ZnO core/shell nanoparticles. The surface morphology, which represented the high agglomeration rate, was investigated using SEM. TEM analysis showed that the sizes of the CuO/ZnO and MgO/ZnO core/shell nanoparticles were 32 nm and 70 nm, respectively. The energy bandgaps were 3.3 eV and 3.1 eV for the CuO/ZnO and MgO/ZnO core/shell nanoparticles.

Keywords: Hybrid nanoparticles, Plasma jets, CuO/ZnO core/shell nanoparticles, MgO/ZnO core/shell nanoparticles, Structural properties, Optical properties

1. Introduction

Nanomaterials have one or more nanometer dimensions (≤100 nm) [1]. Nanomaterials have received significant attention due to their unique properties compared to their bulk counterparts. NPs have small sizes, large surface areas, and unique chemical and physical properties that make them suitable for various applications [2−4]. Recently, metal and metal oxide nanoparticles have attracted great attention among essential materials due to their improved properties, leading to various applications in various fields [5,6]. These materials have widely been studied in various fields such as electronics and catalysis [5]. Among them, oxide metal nanoparticles ZnO, CuO, MgO, etc. Zinc oxide (ZnO) is a multifunctional material due to its high thermal stability and nontoxic nature [6−8].

In contrast, copper oxide (CuO) nanoparticles have been widely used in catalysis, solar energy, electricity, batteries, gas sensors, and organic dye degradation [9]. In recent years, it has been found that surface coating with various semiconductors can significantly improve the characteristics of nanoparticles. There are few reports that have been published related to manufacturing of metal oxide nanocomposites [6,10], with different methods such as ZnO/CuO by one-pot green synthesis [11], MgO/CuO by chemical method [12], Co_3O_4−ZnO by microwave method [13] etc.

Scientists have developed a new class of nanoparticles called hybrid nanoparticles, which are well-organized nanomaterials that contain two, three, or more single nano component types. Core/shell NPs are hybrid nanoparticles called core/shell, core−shell, or core@shell nanoparticles. Core/shell nanoparticles consist of two or more nanomaterials.

Received 16 November 2021; revised 19 January 2022; accepted 24 January 2022.
Available online 1 May 2022.

* Corresponding author at:
E-mail address: raghad.almaliki@uomustansiriyah.edu.iq (R.S. Mohammed).

https://doi.org/10.33640/2405-609X.3225

One nanomaterial acts as the core, and the other nanomaterial coated the core's surface is called the shell [14,15].

Nanoparticles for various materials have been produced using physical and chemical techniques [16]. Nanoparticles can be prepared using various methods such as pulsed laser deposition, sol–gel preparation, chemical coprecipitation, thermal decomposition, hydrothermal methods, etc. [17]. Recently, Plasma jets technology and microwave have gained significant attention as a leading "green technologies" method for nanomaterial synthesis [18,19]. Plasma jets technology has several benefits and advantages, such as environmental friendliness, low cost, and no requirement for expensive equipment [20]. The key to this application is the variety of reactive oxygen and nitrogen species (RONS) created by non-thermal atmospheric pressure plasma sources [21]. Plasma liquid interactions are essential in creating nanomaterials because plasma-generated RONS change the chemical composition of a liquid. During plasma–liquid interactions, the major types of RONS that are formed include hydroxyl radical, hydrogen peroxide, superoxide, ozone, singlet oxygen, nitric oxide, etc. [22]. This work studied the structural properties of CuO/ZnO and MgO/ZnO core/shell nanoparticles. Also were investigated the optical characteristics of these nanoparticles synthesized by plasma jets.

2. Materials and methods

To synthesize hybrid CuO/ZnO and MgO/ZnO core/shell nanoparticles, we used copper foil, magnesium wire, and a zinc sheet with a purity content of 99.99%, purchases from (THE BRITISH DRUG HOUSES LTD./LONDON, Manufactured in England, 652247/470611). As shown in Fig. 1, the experimental setup consisted of a high voltage DC power supply (20 kV) and a stainless steel tube that acted as the cathode. At the same time, copper foil, magnesium wire, or a zinc sheet were used as the anodes, which were immersed in a glass beaker containing 5 ml of deionized water. Ar gas with a purity of 99.99% was used as the gas discharge, and the gas flow was fixed at 2 (L/min) using a flowmeter to control the gas flow. The plasma jet propagated across the air, and the distance between the plasma jet nozzle and the surface of the deionized water was about 2 cm. The plasma treatment of the metal in the liquid lasted for 5 min. The color change in the early time of the reaction indicated that nanomaterials were obtained. The synthesis of CuO/ZnO and MgO/ZnO core/shell nanoparticles was carried out via two steps. The first step included the synthesis of the CuO and MgO cores NPs. The second step included synthesizing the ZnO shell NPs around the CuO and MgO cores NPs. A UV–Vis–NIR Metertech dual-beam spectrometer was used to record the UV–vis absorption spectra of the samples in the 200–900 nm wavelength range. The characterization of the synthesized CuO/ZnO and MgO/ZnO core/shell nanoparticles was examined by techniques, including XRD (XPERT PAANALTICAL PHILLIPS HOLLAND), SEM, EDS (TESCN MIRA3 FRENCH), and TEM, were carried out in Iran at the University of Kashan.

3. Results and discussion

3.1. XRD analyses

The crystal structure and phase purity of the CuO/ZnO and MgO/ZnO core/shell nanoparticles synthesized with the atmospheric plasma jets (APJs) technique was confirmed by the X-ray diffraction (XRD) analysis by comparing the ZnO, CuO, and MgO diffraction angles (2θ°) with the JCPDS card number in the literature.

The XRD pattern was recorded in a 2θ° angle ranging from 25° to 70° for the CuO/ZnO core/shell nanoparticles, as shown in Fig. 2. The CuO/ZnO core/shell nanoparticles XRD pattern revealed diffraction peaks at 31.7° and 56.57°, which were related to the ZnO structure and indexed to the Miller indices of (100) and (112), respectively. This matched with the (JCPDS No: 36–1451) ZnO hexagonal wurtzite structure. Moreover, the smaller peaks at the diffraction angles of 36.2° and 62.6° were found to be related to CuO crystal planes of (111) and (−113), respectively, and the diffraction peaks of the CuO corresponded well to the monoclinic crystal structure (JCPDS card No. 45–0937).

In contrast, the XRD pattern was recorded with a 2θ° angle in the range from 30° to 60° for the MgO/ZnO core/shell nanoparticles, as shown in Fig. 3. Broad diffraction peaks appeared in the XRD patterns of the MgO/ZnO core/shell nanoparticles at the diffraction positions of 31.40°, 34.1°, 36.3°, 47.7°, and 56.94°. These peaks were related to the ZnO structure and indexed to the Miller indices of (100), (002), (101), (102), and (110), respectively. This matched with the JCPDS No. 36–1451 for the ZnO hexagonal wurtzite structure. The diffraction peaks at the 2θ° positions of 36.1° and 38.13° were found to be related to the (002) and (202) planes, respectively, and these peaks were matched with the JCPDS No. 87–0653, for the creation of the MgO polycrystalline cubic structure.

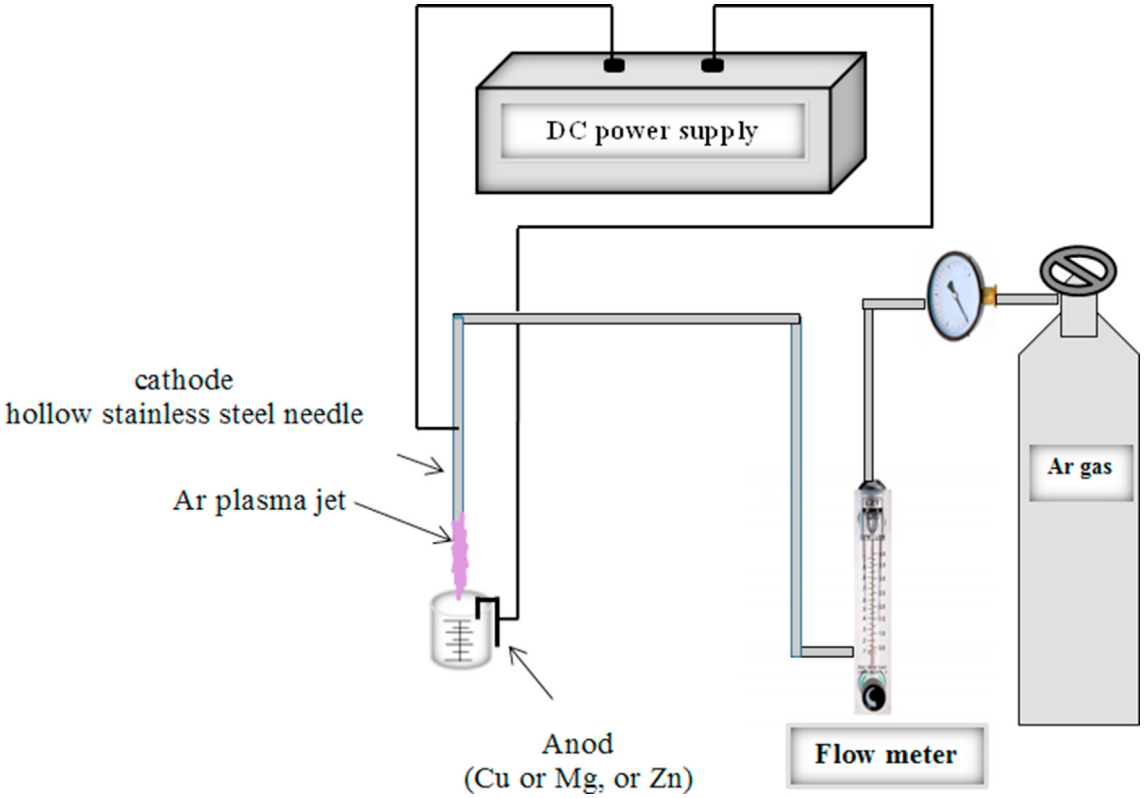

Fig. 1. The experimental setup of CuO/ZnO and MgO/ZnO core/shell NP synthesis by plasma jet.

According to the literature, the XRD pattern of the ZnO nanoparticles revealed an intense (002) peak of diffraction with a wurtzite structure (JCPDS No. 36–1451) at a diffraction angle of 34.4° [23,24]. The ZnO crystal structure was in a thermodynamically stable state when the zinc and oxygen atoms had tetrahedral arrangements. Thus, the presence of the (002) diffraction peak confirmed that the ZnO maintained a wurtzite structure with a hexagonal unit cell after the ZnO shell was created around the surface of the CuO core nanoparticles.

There were no other peaks related to the secondary phases for the CuO, MgO, or ZnO in the XRD pattern of the CuO/ZnO and MgO/ZnO

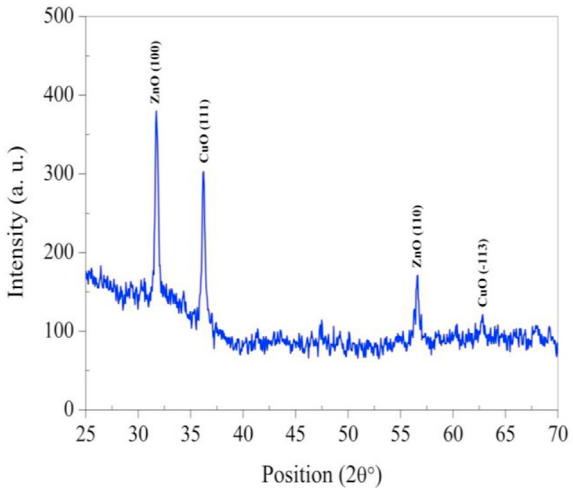

Fig. 2. XRD pattern for CuO/ZnO core/shell NPs synthesis by plasma jet.

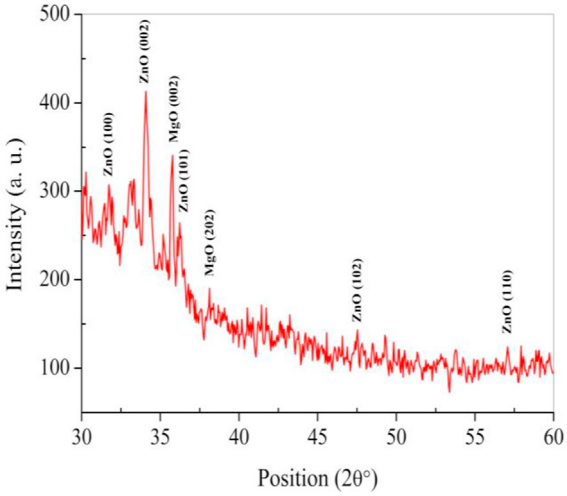

Fig. 3. XRD pattern for MgO/ZnO core/shell NP synthesis by plasma jet.

nanoparticles, indicating the purity of the created nanoparticles. Moreover, the slight shifts in the diffraction angles of the CuO, MgO, and ZnO nanoparticles in comparison to the standard data showed that the characteristic peaks of the CuO, MgO, and ZnO changed. The occurrence of a distinct line broadening in the diffraction peaks confirmed the formation of nanometer-sized particles [25,26], indicating that CuO/ZnO and MgO/ZnO core/shell NPs were successfully formed.

The Debye-Scherer Equation (1) was used to measure the nanoparticle crystallite sizes of the CuO/ZnO and MgO/ZnO core/shell nanoparticles [27]:

$$D\ (^{\circ}A) = k\lambda/\beta\cos\theta \quad (1)$$

In the expression, D is the crystallite size, k: is the Scherer's constant ($k = 0.9$), λ is the X-ray wavelength (1.540 Å), and β is the full width at half maximum (FWHM) of the peaks at the θ diffracting angle from the Bragg's angle position.

The average crystalline sizes of the CuO/ZnO and MgO/ZnO core/shell NPs were 28 nm and 36 nm, respectively.

The intensity of the CuO and MgO peaks was lower than that of the ZnO diffraction peaks, and this corresponded to the EDX analysis results. The average crystallite size decreased as the concentration of CuO and MgO decreased, indicating the creation of nanoparticles with small sizes. The minor alterations suggested that modifying the ZnO with CuO and MgO had an impact on its structure. The lattice distortion generated by the radius difference between the Zn^{+2}, Cu^{+2}, and Mg^{+2} ions reduced the crystallite size [25,28].

3.2. SEM analyses

The morphology of the CuO/ZnO and MgO/ZnO core/shell nanoparticles synthesized by the plasma jets technique was investigated using scanning electron microscopy (SEM) images. The SEM images demonstrated that the created particles had a nanoparticle nature and morphology, that the nanoparticles agglomerated, and that complete separation was not achieved. The shapes of the CuO/ZnO core/shell NPs synthesized by plasma jets had the appearance of overlapped sheets, as shown in Fig. 4, and the MgO/ZnO core/shell NPs were spindle-shaped, as shown in Fig. 5. The presence of some large size grains and the aggregation of the NPs could be attributed to the increased surface areas and surface energies of the CuO and MgO core NPs [25]. Because of the higher surface area to volume ratio, the nanoparticles were held together or agglomerated by the attractive physical forces between them.

3.3. EDX analyses

To the knowledge of the synthesized samples chemical composition, the energy dispersive X-ray (EDX) analysis was used. The presence of peaks related to Cu, Zn, and O elements in the CuO/ZnO core/shell nanoparticles was confirmed by the EDX spectrum, as shown in Fig. 6., and Mg, Zn, and O elements in the MgO/ZnO core/shell nanoparticles, as shown in Fig. 7. The composition of the core/shell NPs, as confirmed by the EDX analysis, was pure, with no other impurity elements present. The plasma jet technique successfully synthesized CuO/ZnO and MgO/ZnO core/shell nanoparticles, as evidenced by the EDX spectra, confirming the verified XRD result. The percentages of the compositions (weight % and atomic %) of the Cu, Mg, Zn, and O in the CuO/ZnO and MgO/ZnO core/shell NPs are stated in Fig. 6 and Fig. 7.

3.4. TEM analysis

A transmission electron microscopy (TEM) analysis was carried out to confirm the synthesis of the core/shell nanoparticles with atmospheric plasma jets due to the ability to measure the thickness and the distance between the core and shells. The information relevant to the shape, size, and aggregation was also obtained from TEM analysis. Additionally, the TEM analysis demonstrated that there were two different regions. The dark inner part represented the core, and the shiny part surrounding the dark region represented the shell, confirming the synthesis of CuO/ZnO and MgO/ZnO core/shell nanoparticles. The Image J software program was used to analyze the TEM image to calculate the particle sizes. The average size of the CuO/ZnO core/shell NPs was 32 nm, as indicated in the size of particles histogram in Fig. 8b, and the MgO/ZnO core/shell NPs had an average size of 70 nm, as shown in the size of particles histogram in Fig. 9b.

3.5. Optical properties

The optical absorption properties of hybrid CuO/ZnO, MgO/ZnO core/shell nanoparticles generated using the atmospheric plasma jets (APJs) technique were characterized using UV–vis spectroscopy. The optical characterization of the nanoparticles provided information about physical properties such as

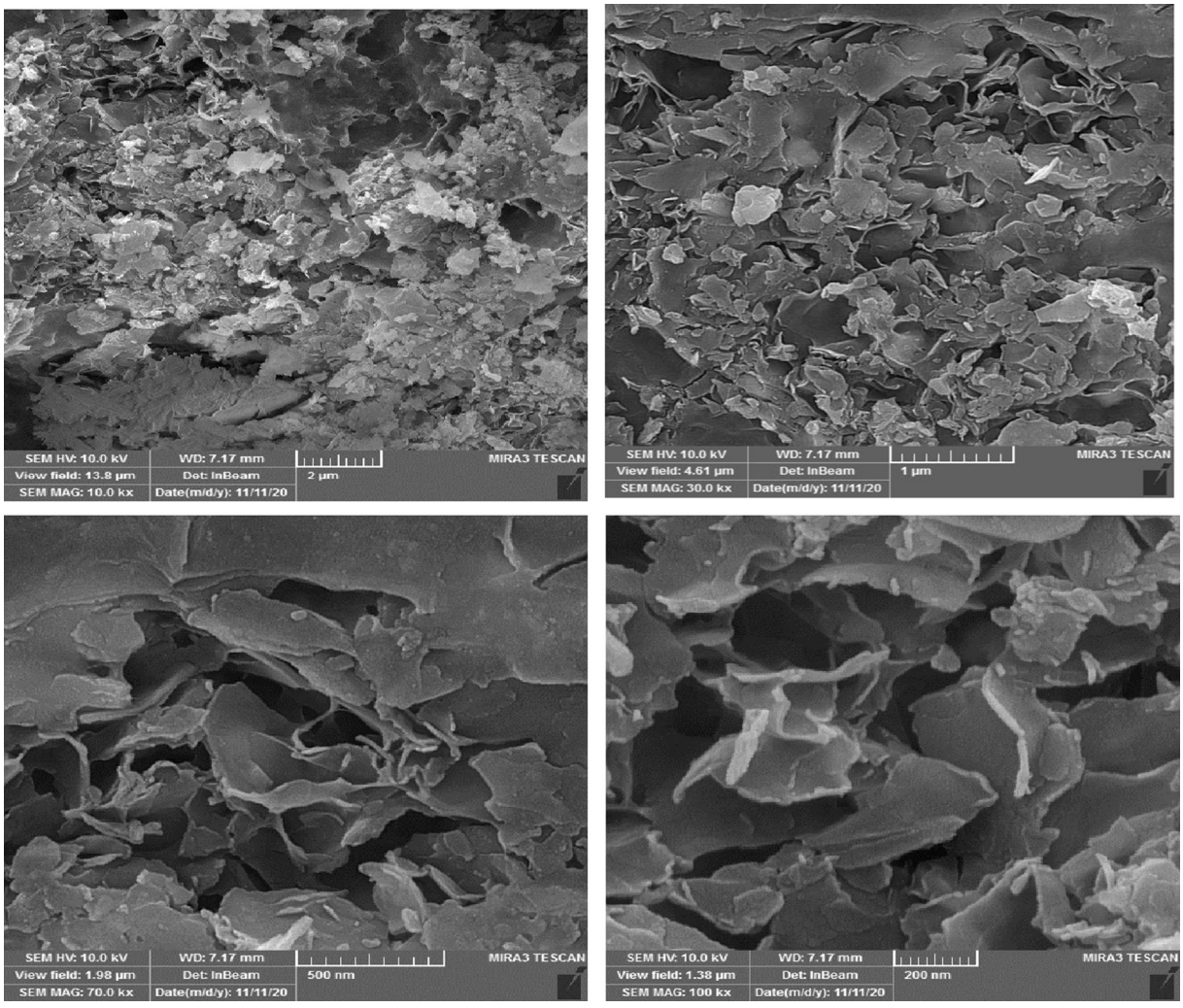

Fig. 4. SEM images of CuO/ZnO core/shell NPs synthesized by plasma jet technique at different magnification.

absorbance and bandgap energy. A UV−vis spectrophotometer is based on sample light absorption. The bandgap is the key optical parameter. Plotting the experimental absorbance data is a common method to measure the optical band gap of nanoparticles. The bandgap was measured directly from λ_{cut} by applying Planck's law, as shown in Equation (2) [27]:

$$E_g = hc/\lambda_{cut} = 1240/\lambda_{cut} \quad (2)$$

where E_g is the optical energy gap, h=$(6.626 \times 10^{-34}$ J s) is Planck's constant, c = $(3 \times 10^8$ m/s) is the light velocity, and λ_{cut} is the cut-off wavelength corresponding to the optical bandgap. λ_{cut} was determined graphically from the extrapolation of the linear region.

The electronic interactions caused by the ZnO shell that was created on the surface of the CuO core and MgO core nanoparticles were investigated using the UV−vis absorbance measurements of the CuO/ZnO and MgO/ZnO core/shell NPs synthesized with the atmospheric plasma jet technique. At room temperature, UV−vis absorption spectra of CuO/ZnO and MgO/ZnO core/shell nanoparticles as a function of wavelength are shown in Figs. 10 and 11. Broad absorption peaks were observed for CuO/ZnO core/shell NPs in the wavelength range of 300 nm to 400 nm, and 300 nm to 500 nm for MgO/ZnO core/shell NPs.

Fig. 10 shows the optical absorption of the CuO/ZnO core/shell NPs. We observed that the absorption edge of these nanoparticles exhibited a blue shift due to the overall size. The total size of the core/shell was greater than the core size after a shell was created around the core surface. This blue shift behaviour of the CuO/ZnO core/shell NPs was expected to increase the optical band gap value (E_g = 3.01 eV).

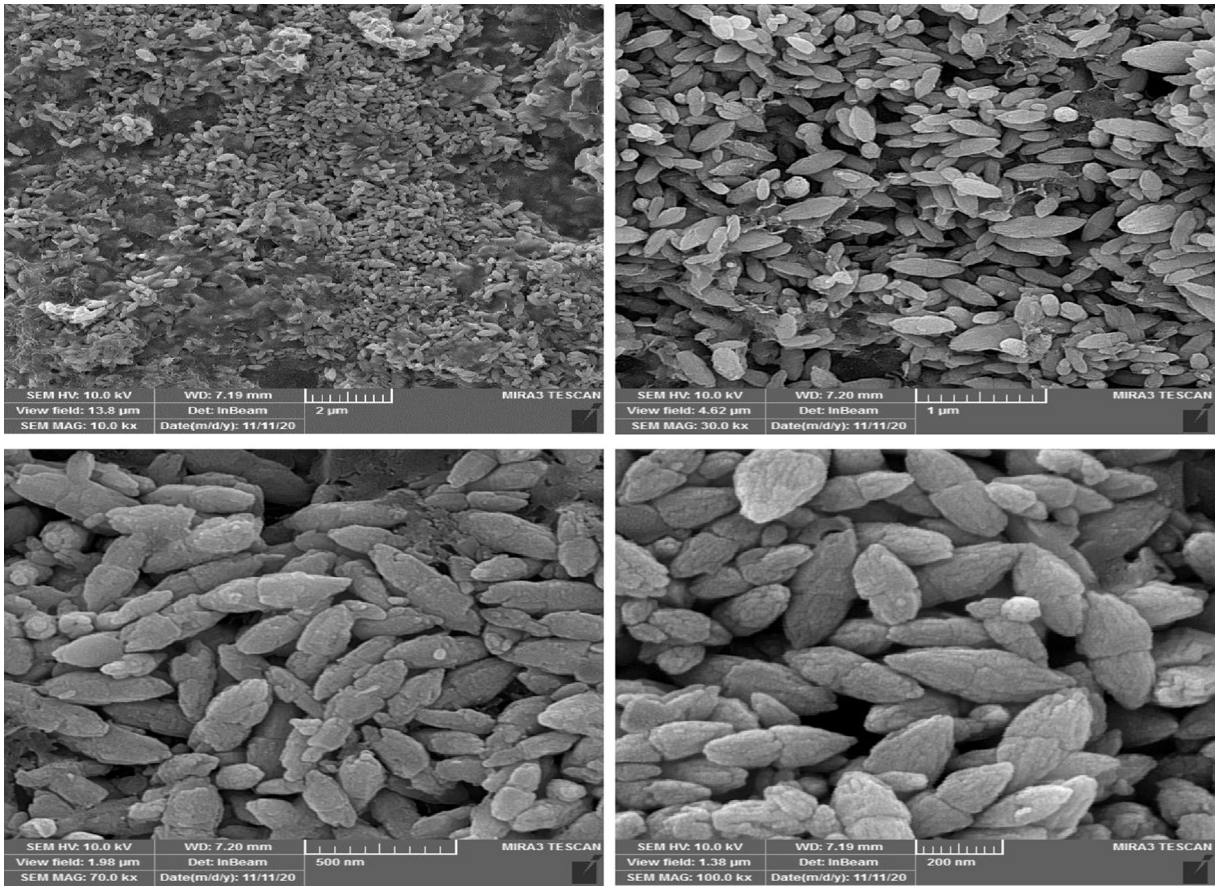

Fig. 5. SEM images of MgO/ZnO core/shell NPs synthesized by plasma jet technique at different magnification.

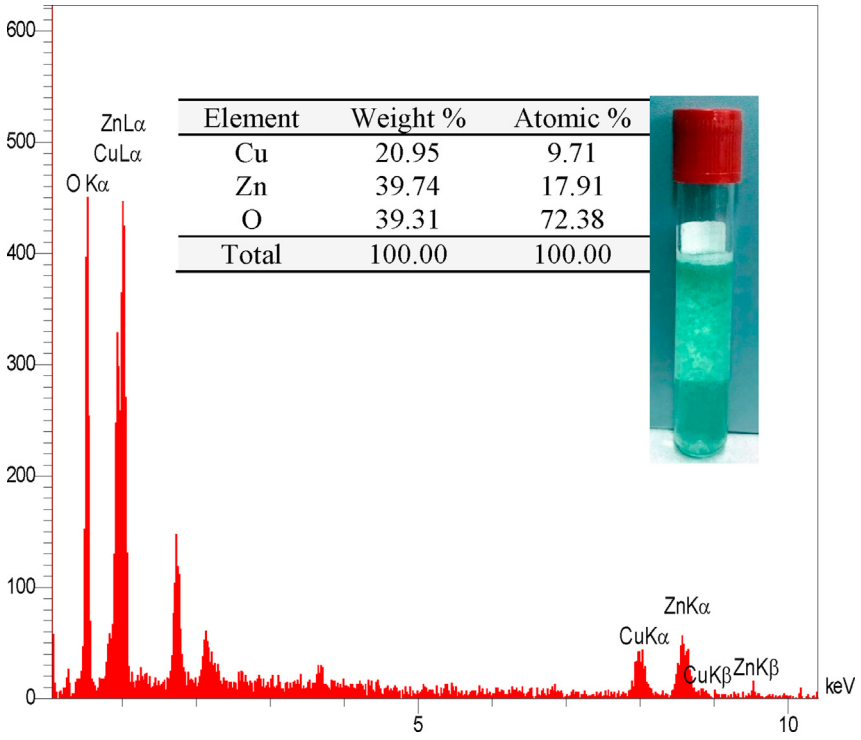

Fig. 6. EDX spectra of the CuO/ZnO core/shell nanoparticles synthesized by plasma jet.

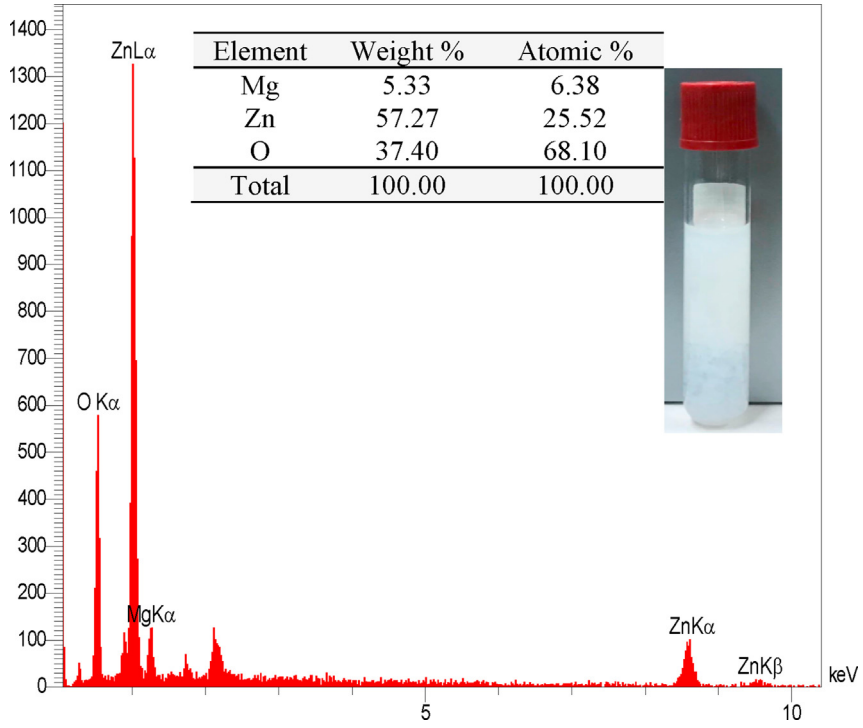

Fig. 7. EDX spectra of the MgO/ZnO core/shell nanoparticles synthesized by plasma jet.

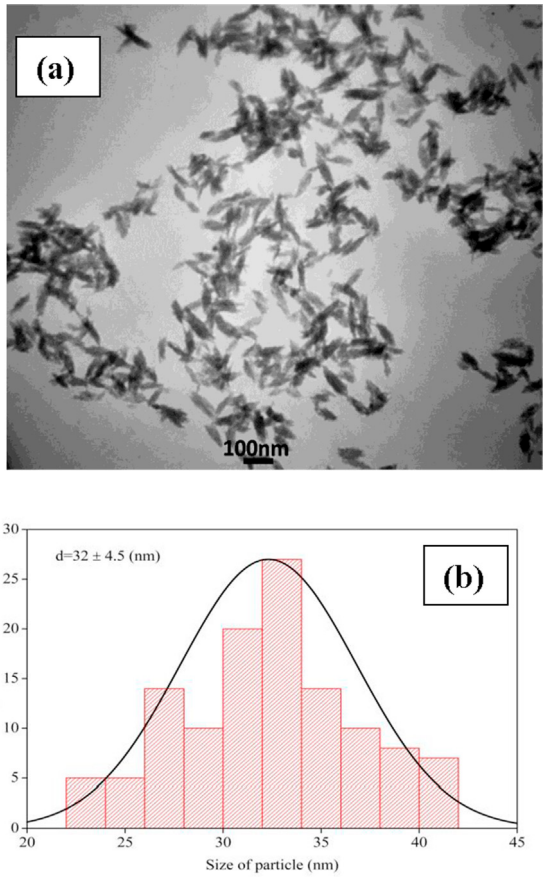

Fig. 8. (a). TEM image of CuO/ZnO core/shell NPs, (b). Size of particles histogram of CuO/ZnO core/shell NPs synthesized by plasma jet.

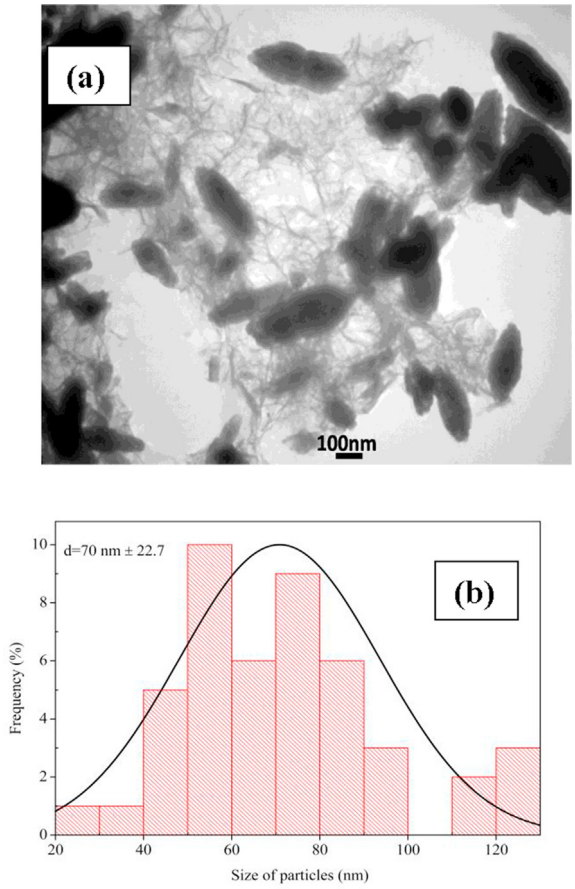

Fig. 9. (a). TEM image of MgO/ZnO core/shell NPs, (b). Size of particles histogram of MgO/ZnO core/shell NPs synthesized by plasma jet.

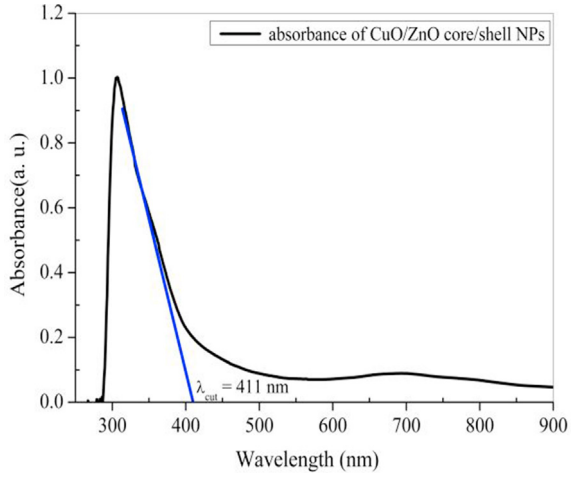

Fig. 10. CuO/ZnO core/shell nanoparticles optical absorption spectra.

In contrast, it was noted from Fig. 11 that the MgO/ZnO core/shell NPs' absorption edge was shifted to a longer wavelength (redshift), this redshift behaviour was expected to decrease the optical bandgap (E_g) value. According to Kumar et al. (2013) [29], the aggregation in the samples might have been responsible for the redshift. For the MgO/ZnO core/shell NPs, the bandgap energies were 2.8 eV. This result was less than reported in the literature review [30,31].

This behaviour could have been due to the combination of ZnO ions in the MgO lattice. The outcome was consistent with Maruthai et al. (2018) [31]. The MgO/ZnO core/shell nanoparticles showed a significant absorption at wavelengths below 550 nm. This was due to the higher absorption of the incident photon energy by the molecules in the lower energy levels, which caused the molecules to be excited to higher energy levels. The increase in the absorbance of the MgO/ZnO core/shell NPs compared with the MgO and ZnO NPs reported in the previous literature might have been caused by various factors such as particle size, oxygen deficiency, or defects in the grain structure [25,32].

Based on the absorbance spectra, the absorption coefficients of the CuO/ZnO and MgO/ZnO core/shell nanoparticles were determined graphically by applying Tauc's relationship for direct transition, as shown in Equation (3) [33]:

$$(\alpha h\upsilon)^r = A(h\upsilon - E_g) \quad (3)$$

Where α is the absorption coefficient, h is Planck's constant, υ is the incident photon frequency, A is a constant equal to 0.9, E_g is the optical energy gap, and r is a value that depends on the nature of the transition type ($r = 2$) for the allowed direct transition. Plotting a graph between the photon energy ($h\nu$) and $(\alpha h\nu)^r$ is a common method for determining a bandgap by extrapolating the straight line to the axis intercept, as shown in Figs. 12 and 13.

For the CuO/ZnO core/shell NPs, the value of E_g was 3.3 eV. This result agreed well with that of Li

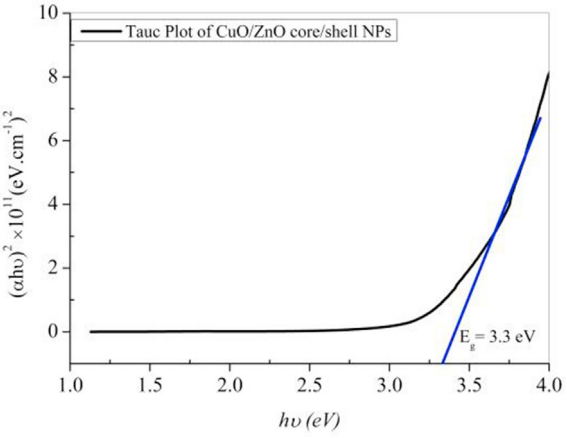

Fig. 12. Optical band gap energy for CuO/ZnO core/shell NPs.

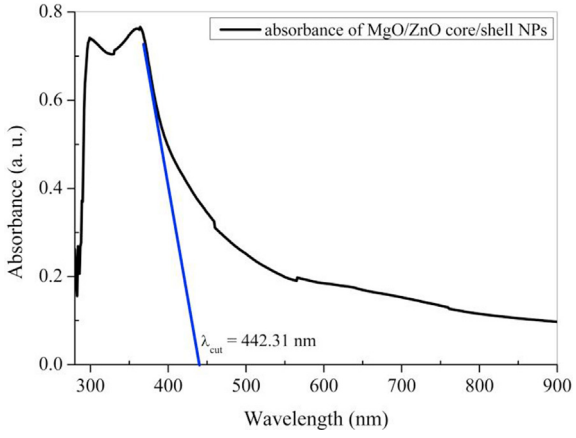

Fig. 11. MgO/ZnO core/shell nanoparticles optical absorption spectra.

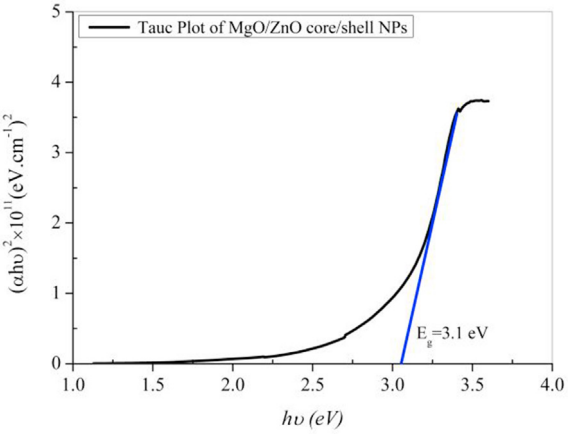

Fig. 13. Optical bandgap energy for MgO/ZnO core/shell NPs.

et al. [34]. The E_g of the CuO/ZnO NPs was found higher than for the CuO NPs in the reported literature. The increased energy gap between the conduction and the valence bands of the CuO/ZnO core/shell NPs could be attributed to the decreased crystalline size. Hence, it might be concluded that the ZnO shell NPs extended the energy gap of the CuO NPs [35]. Furthermore, the bandgap value for the MgO/ZnO NPs was 3.1 eV, and this result was in good agreement with that of Shi et al. (2015) [36].

4. Conclusion

The plasma jet technique was used to successfully synthesize CuO/ZnO and MgO/ZnO core/shell NPs. This synthesis technique provided nanoparticles with high purity according to XRD and EDS analyses. The XRD results showed that the nanoparticles were purely crystalline, and the average crystallite sizes were 28 nm and 35.58 nm for the CuO/ZnO and MgO/ZnO core/shell NPs, respectively. The SEM and TEM results exhibited the formation of aggregated small particles with a mean diameter of 32.2 nm for the CuO/ZnO core/shell NPs and 70 nm for the MgO/ZnO core/shell NPs. The results obtained from our study demonstrated that the CuO/ZnO and MgO/ZnO core/shell NPs exhibited excellent optical properties for the absorption and bandgap, and the NPs could be more active in visible light for various applications such as photovoltaics.

Acknowledgements

This study is supported by Plasma Physics Lab., Physics Department, College of Science, University of Baghdad.

References

[1] R.G. Chaudhuri, S. Paria, Core/shell nanoparticles: classes, properties, synthesis mechanisms, characterization, and applications, Chem Rev 112 (4) (2011) 2373–2433, https://doi.org/10.1021/cr100449n.
[2] Q. Jiao, L. Li, Q. Mu, Q. Zhang, Immunomodulation of nanoparticles in nanomedicine applications, BioMed Res Int 2014 (2014) 1–19, https://doi.org/10.1155/2014/426028.
[3] N.K. Kaushik, N. Kaushik, N.N. Linh, B. Ghimire, A. Pengkit, J. Sornsakdanuphap, S.J. Lee, E.H. Choi, Plasma and nanomaterials: fabrication and biomedical applications, Nanomaterials 9 (1) (2019) 98, https://doi.org/10.3390/nano9010098.
[4] K. Zhou, X. Zhou, J. Liu, Z. Huang, Application of magnetic nanoparticles in petroleum industry: a review, J Petrol Sci Eng 188 (2020) 106943, https://doi.org/10.1016/j.petrol.2020.106943.
[5] Y. Lee, B. Bora, S. Yap, C. Wong, Effect of ambient air pressure on synthesis of copper and copper oxide nanoparticles by wire explosion process, Curr Appl Phys 12 (1) (2012) 199–203, https://doi.org/10.1016/j.cap.2011.06.001.
[6] P. Mahajan, A. Singh, R. Datt, V. Gupta, S. Arya, Realization of inverted organic solar cells by using sol-gel synthesized ZnO/Y2O3 core/shell nanoparticles as electron transport layer, IEEE J Photovolt 10 (6) (2020) 1744–1749, https://doi.org/10.1109/JPHOTOV.2020.3014874.
[7] S. Arya, P. Mahajan, S. Mahajan, A. Khosla, R. Datt, V. Gupta, S.-J. Young, S.K. Oruganti, Review—influence of processing parameters to control morphology and optical properties of sol-gel synthesized ZnO nanoparticles, ECS J Solid State Sci Technol 10 (2) (2021), 023002, https://doi.org/10.1149/2162-8777/abe095.
[8] A. Indriyani, Y. Yulizar, R. Tri Yunarti, D. Oky Bagus Apriandanu, R. Marcony Surya, One-pot green fabrication of BiFeO3 nanoparticles via Abelmoschus esculentus L. leaves extracts for photocatalytic dye degradation, Appl Surf Sci 563 (2021) 150113, https://doi.org/10.1016/j.apsusc.2021.150113.
[9] D.O.B. Apriandanu, Y. Yulizar, Tinospora crispa leaves extract for the simple preparation method of CuO nanoparticles and its characterization, Nano-Struct. Nano-Objects 20 (2019) 100401, https://doi.org/10.1016/j.nanoso.2019.100401.
[10] D.O.B. Apriandanu, Y. Yulizar, CuO-bentonite-gold nanocomposites: facile green preparation and their characterization, Mater Lett 284 (2021) 128911, https://doi.org/10.1016/j.matlet.2020.128911.
[11] Y. Yulizar, R. Bakri, D.O.B. Apriandanu, T. Hidayat, ZnO/CuO nanocomposite prepared in one-pot green synthesis using seed bark extract of Theobroma cacao, Nano-Struct Nano-Objects 16 (2018) 300–305, https://doi.org/10.1016/j.nanoso.2018.09.003.
[12] K. Kaviyarasu, C. Maria Magdalane, K. Anand, E. Manikandan, M. Maaza, Synthesis and characterization studies of MgO:CuO nanocrystals by wet-chemical method, Spectrochim Acta Mol Biomol Spectrosc 142 (2015) 405–409, https://doi.org/10.1016/j.saa.2015.01.111.
[13] M. Hassanpour, H. Safardoust-Hojaghan, M. Salavati-Niasari, Degradation of methylene blue and Rhodamine B as water pollutants via green synthesized Co_3O_4/ZnO nanocomposite, J Mol Liq 229 (2017) 293–299, https://doi.org/10.1016/j.molliq.2016.12.090.
[14] M.B. Gawande, A. Goswami, T. Asefa, H. Guo, A.V. Biradar, D.-L. Peng, R. Zboril, R.S. Varma, Core–shell nanoparticles: synthesis and applications in catalysis and electrocatalysis, Chem Soc Rev 44 (21) (2015) 7540–7590, https://doi.org/10.1039/C5CS00343A.
[15] M. Khatami, H.Q. Alijani, I. Sharifi, Biosynthesis of bimetallic and core–shell nanoparticles: their biomedical applications–a review, IET Nanobiotechnol 12 (7) (2018) 879–887, https://doi.org/10.1049/iet-nbt.2017.0308.
[16] Y.R. Parauha, V. Sahu, S. Dhoble, Prospective of combustion method for preparation of nanomaterials: a challenge, Mater Sci Eng B 267 (2021) 115054, https://doi.org/10.1016/j.mseb.2021.115054.
[17] R. Sagheer, S.T. Khadija, Z.N. Kayani, S. Riaz, Structural, optical and magnetic properties of ZnO nanoparticles tailored by 'La^{3+}' ions, Optik 244 (2021) 166816, https://doi.org/10.1016/j.ijleo.2021.166816.
[18] L.N. Nguyen, P. Lamichhane, E.H. Choi, G.J. Lee, Structural and optical sensing properties of nonthermal atmospheric plasma-synthesized polyethylene glycol-functionalized gold nanoparticles, Nanomaterials 11 (7) (2021) 1678, https://doi.org/10.3390/nano11071678.
[19] J. Wojnarowicz, T. Chudoba, W. Lojkowski, A review of microwave synthesis of zinc oxide nanomaterials: reactants, Process Parameter Morpholog Nanomater 10 (6) (2020) 1086, https://doi.org/10.3390/nano10061086.
[20] M. Sajjad, I. Ullah, M. Khan, J. Khan, M.Y. Khan, M.T. Qureshi, Structural and optical properties of pure and copper doped zinc oxide nanoparticles, Results Phys 9 (2018) 1301–1309, https://doi.org/10.1016/j.rinp.2018.04.010.
[21] T. Von Woedtke, S. Reuter, K. Masur, K.D. Weltmann, Plasmas for medicine, Phys Rep 530 (4) (2013) 291–320, https://doi.org/10.1016/j.physrep.2013.05.005.

[22] B. Ghimire, J. Sornsakdanuphap, Y.J. Hong, H.S. Uhm, K.D. Weltmann, E.H. Choi, The effect of the gap distance between an atmospheric-pressure plasma jet nozzle and liquid surface on OH and N_2 species concentrations, Phys Plasmas 24 (7) (2017), 073502, https://doi.org/10.1063/1.4989735.
[23] M. Goswami, N.C. Adhikary, S. Bhattacharjee, Effect of annealing temperatures on the structural and optical properties of zinc oxide nanoparticles prepared by chemical precipitation method, Optik 158 (2018) 1006–1015, https://doi.org/10.1016/j.ijleo.2017.12.174.
[24] M.S. Nadeem, T. Munawar, F. Mukhtar, M.N. Ur Rahman, M. Riaz, F. Iqbal, Enhancement in the photocatalytic and antimicrobial properties of ZnO nanoparticles by structural variations and energy bandgap tuning through Fe and Co co-doping, Ceram Int 47 (8) (2021) 11109–11121, https://doi.org/10.1016/j.ceramint.2020.12.234.
[25] P. Mahajan, A. Singh, S. Arya, Improved performance of solution processed organic solar cells with an additive layer of sol-gel synthesized ZnO/CuO core/shell nanoparticles, J Alloys Compd 814 (2020) 152292, https://doi.org/10.1016/j.jallcom.2019.152292.
[26] A. Singh, A. Ahmed, A. Sharma, C. Sharma, S. Paul, A. Khosla, V. Gupta, S. Arya, Promising photocatalytic degradation of methyl orange dye via sol-gel synthesized Ag–CdS@Pr-TiO2 core/shell nanoparticles, Phys B Condens Matter 616 (2021) 413121, https://doi.org/10.1016/j.physb.2021.413121.
[27] A. Ali, Y. Rammah, R. El-Mallawany, D. Souri, FTIR and UV spectra of pentaternary borate glasses, Measurement 105 (2017) 72–77, https://doi.org/10.1016/j.measurement.2017.04.010.
[28] K. Pradeev raj, K. Sadaiyandi, A. Kennedy, S. Sagadevan, Z.Z. Chowdhury, M.R.B. Johan, F.A. Aziz, R.F. Rafique, R.T. Selvi, R. Rathina bala, Influence of Mg doping on ZnO nanoparticles for enhanced photocatalytic evaluation and antibacterial analysis, Nanoscale Res Lett 13 (229) (2018) 1–13, https://doi.org/10.1186/s11671-018-2643-x.
[29] S.S. Kumar, P. Venkateswarlu, V.R. Rao, G.N. Rao, Synthesis, characterization and optical properties of zinc oxide nanoparticles, Int Nano Lett 3 (30) (2013) 1–6, https://doi.org/10.1186/2228-5326-3-30.
[30] S. Klubnuan, P. Amornpitoksuk, S. Suwanboon, Structural, optical and photocatalytic properties of MgO/ZnO nanocomposites prepared by a hydrothermal method, Mater Sci Semicond 39 (2015) 515–520, https://doi.org/10.1016/j.mssp.2015.05.049.
[31] J. Maruthai, A. Muthukumarasamy, B. Baskaran, Optical, biological and catalytic properties of ZnO/MgO nanocomposites derived via Musa paradisiaca bract extract, Ceram Int 44 (11) (2018) 13152–13160, https://doi.org/10.1016/j.ceramint.2018.04.138.
[32] S. Tachikawa, A. Noguchi, T. Tsuge, M. Hara, O. Odawara, H. Wada, Optical properties of ZnO nanoparticles capped with polymers, Materials 4 (6) (2011) 1132–1143, https://doi.org/10.3390/ma4061132.
[33] H. Gayitri, M. AL-Gunaid, A. Gnana Prakash, Investigation of triplex CaAl2ZnO5 nanocrystals on electrical permittivity, optical and structural characteristics of PVA nanocomposite films, Polym Bull 77 (2020) 5005–5026, https://doi.org/10.1007/s00289-019-03069-3.
[34] H. Li, L. Zhu, M. Xia, N. Jin, K. Luo, Y. Xie, Synthesis and investigation of novel ZnO–CuO core-shell nanospheres, Mater Lett 174 (2016) 99–101, https://doi.org/10.1016/j.matlet.2016.03.079.
[35] M. Verma, V. Kumar, A. Katoch, Sputtering based synthesis of CuO nanoparticles and their structural, thermal and optical studies, Mater Sci Semicond 76 (2018) 55–60, https://doi.org/10.1016/j.mssp.2017.12.018.
[36] Z.F. Shi, Y.T. Zhang, X.J. Cui, S.W. Zhuang, B. Wu, J.Y. Jiang, X.W. Chu, X. Dong, B.L. Zhang, G.T. Du, Epitaxial growth of vertically aligned ZnO nanowires for bidirectional direct-current driven light-emitting diodes applications, CrystEngComm 17 (2015) 40–49, https://doi.org/10.1039/c4ce01788a.